Article

Critical assessment of the bonded single lap joint exposed to cyclic tensile loading

Murat Demiral[1,*], Fethi Abbassi[1] , Abolfazl Zahedi[2] and Salih Akpınar[3]

[1] College of Engineering and Technology, American University of the Middle East, Kuwait
[2] School of Engineering and Sustainable Development, De Montfort University, Leicester, LE1 9BH, UK
[3] Dept. Of Mechanical Eng., Erzurum Technical University, Erzurum, Turkey
* Correspondence: E-mail: murat.demiral@aum.edu.kw

Abstract: Single shear or single lap joints are the most prevalent type of adhesive joints used in advanced engineering applications, where they are exposed to fatigue loadings in their services. Although their mechanical performances under static loading have been investigated extensively, the studies related to the fatigue performances were limited. For that purpose, single lap joint's (SLJ's) reaction to fatigue tensile loading was studied by varying the adherend thickness (3 mm to 6 mm) and fatigue load (3250 N to 1500 N). ABAQUS/Standard was used to create its advanced FE model. To represent the progressive damage in the adhesive layer, the fatigue damage model via the Paris Law, which links the rate of the crack expansion to the strain energy release rate (SERR), was integrated into the cohesive zone model having a bi-linear traction–separation characteristics. The model was written in a UMAT subroutine. The developed model was validated using experimental data from the literature. The crack initiation cycle (N_i), the failure cycle (N_f), the fatigue load limit, the strain energy release rate, the crack propagation rate, and variation of stress components with their dependency to design parameters were investigated in depth. It was found that the service life of the SLJs with thicker adherends was more responsive to the amount of stress applied. When exposed to lesser loads, the SLJs' life span changed more noticeably.

Keywords: Bonded joint; Fatigue loading; Strain energy release rate; Paris Law; Cohesive zone model; Service life

1. Introduction and motivation

Advanced engineering applications are increasingly using bonded joints as an alternative to more conventional methods including fastening, riveting, bolting and welding [1]. Uniform stress distribution along the width, a reduced amount of stress concentrations, lower structural weight as well as better fatigue and damping characteristics are among the advantages of the bonded joints. The complexities related to their productions such as surface preparation, manufacturing and curing conditions as well as the extreme environmental conditions are some of the challenges in this field. An increasing amount of research on these bonding types enabled bonded joints to become stronger than the parent materials' greater ductility, peel and shear strengths till failure.

The most common kind of adhesive joints utilized in airplane applications are single shear or single lap joints. Even though these joint types are the weakest, they are chosen due to their ease of fabrication and inspection. They are frequently employed in wing ribs and wing spars to wing skin joints, fuselage frames to fuselage skins [2]. Different components of the airplane structure, including the lap joints, are exposed to static loads, but mainly fatigue loadings in their services as a result of repeated flight cycles and frequent use. The dynamic loadings with regular or irregular cyclic loads are also due to environmental effects. For the former loading, many studies were performed in the literature [3-5]. However, few studies were dedicated for the fatigue loading [6]. Among them,

Khoromishad et al. [7] developed a progressive fatigue damage modelling based on a bi-linear traction-separation cohesive zone model for a SLJ. The numerical predictions were consistent with the experimental fatigue response in terms of the life of the SLJ, damage progress and back-face strains. A similar study was performed by Ibrahım et al. [8], where the damage surface concept served as a foundation for the fatigue damage degradation. Quaresimin and Ricotta [9] described the phases of fracture propagation and nucleation that made up the joint lifetime, where the generalized stress intensity factor (SIF) technique was used to model the former one and by incorporating a power law with a Paris-like relationship between the strain energy release rate (SERR) and the rate of crack expansion for the latter. Shahani and Pourhosseini [10] conducted an experimental and numerical analysis of the effect of adherent thickness on the fatigue performance of adhesively bonded thin aluminum single lap joints (SLJ). According to this work, when the adhesive layer thickness increased, the fatigue limit also increased and the likelihood of an adhesive layer failure increased. Experimental research by Sahin and Akpinar [11] examined the impact of adherend thickness on the fatigue strength of adhesively bonded SLJ. Because of the adherend's flexural rigidity and the formed bending moment in the joint, it was discovered that the fatigue load applied to the SLJ resulting in infinite life cycles to increase for thicker adherends. In another study, Katnam et al. [12] created a fatigue damage model with a bi-linear traction-separation response based on a cohesive zone model for a tapered single lap joint using an effective strain-based method. This study looked into how the load ratio affected the way adhesively bonded joint failed. Li et al. [13] used experimental and numerical methods to study the fatigue properties of steel and carbon fiber reinforced plastic laminated SLJs subjected to vibration loads. More studies about traction–separation laws and SLJs can be found elsewhere [14-17].

Understanding its failure mechanisms in terms of damage initiation, progression, as well as the failure sequence of the joint constituents are vital for the development of reliable joint designs. Especially, the crack initiation (N_i) and the failure cycles (N_f), the fatigue load limit, the crack propagation rate, strain energy release rate and failure modes with their dependency to design parameters need to be clarified. However, in none of the above studies, these points were not investigated systematically. This research offers a numerical analysis to assess the fatigue performance of an adhesively-bonded SLJ made of AA2024-T3 aluminum alloy adherends and DP460 structural adhesive and subjected to tensile loading for various adherend thicknesses and fatigue loads. The cohesive zone elements were used in simulations to discretize the adhesive layer. Based on damage mechanics, the rate of fatigue damage was determined, where the damage builds up due to cyclic material weakening. The Paris Law, which links the SERR to the rate of crack formation, was used to calculate the life spent in the propagation phase. To do this, a user-defined UMAT function was employed. The behavior of the adherends was modeled using an elasto-plastic material model. The developed model was validated using experimental data from the literature.

The structure of this work is as follows: The developed FE model is described in Section 2, where a short description of the cohesive zone modeling theory is provided. The results and discussion of the performed parametric analysis are presented in Section 3 after the validation of the numerical model via the experimental data. Section 4 of the paper contains concluding remarks.

2. Numerical modelling

The FE modelling was used to simulate an adhesively-bonded SLJ of aluminum adherends subjected to tensile fatigue loading. (Fig. 1). ABAQUS/Standard was used to run 2D simulations [18].

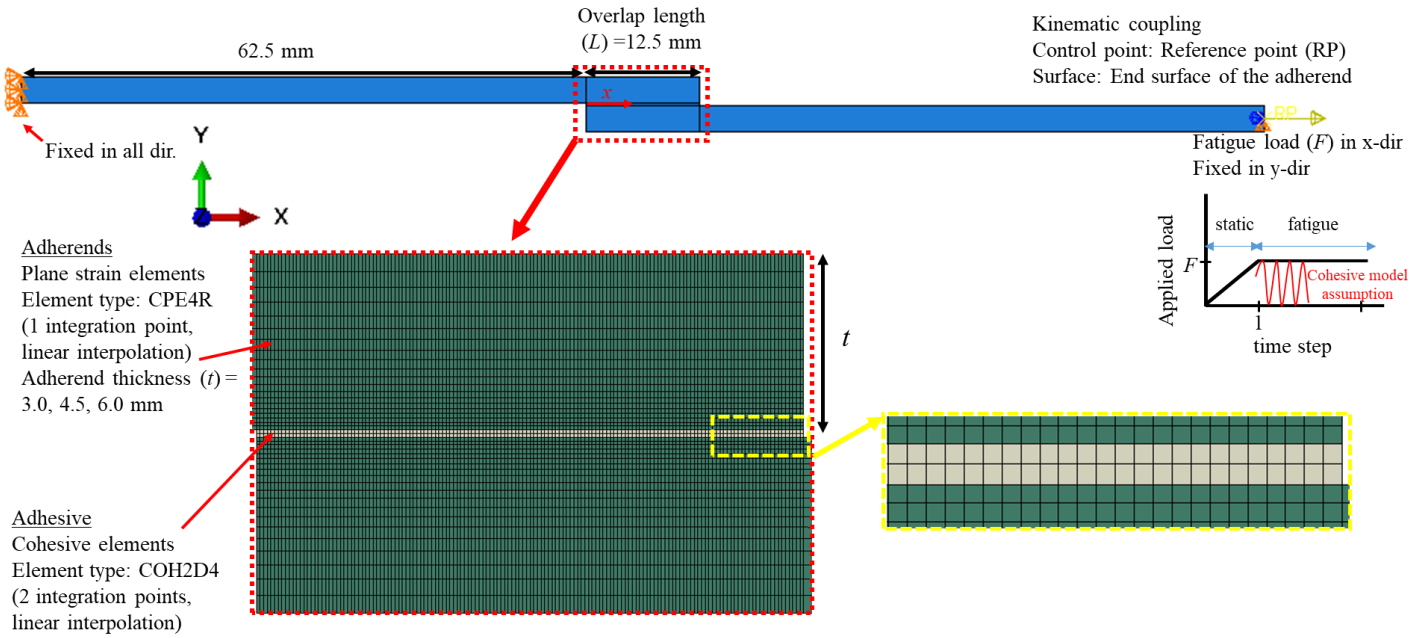

Figure 1. Specifications of the 2D FE model of the SLJ under fatigue tensile loading.

The adherends were represented by 4-node plane strain elements (CPE4R). To examine the increasing degradation in the adhesive layer, using a bilinear traction separation description, four-noded cohesive elements (COH2D4) were employed. A mesh convergency study was performed based on the number of failure cycles and the von-Mises stress value at the left end element of the adhesive layer upon 3.0 kN static tensile load was applied. Three different element sizes along the overlap length in the adhesive layer, 0.10 mm, 0.050 mm and 0.025 mm, were considered. It was noticed that the change in the mentioned stress was 9.4% and 3.1% when the mesh was changed from coarsest mesh into the intermediate size mesh and then intermediate into the finest mesh. As a result, an average element size of 0.050 mm was used in the adhesive layer (see Fig. 1). This mesh size also predicted the number of failure cycles with almost the same accuracy that the finest mesh predicted (their difference was also less than 4.0%). On the other hand, a finer mesh with a single bias ratio of 2 (in the direction of the connecting region) was used to discretize the adherend material. Overall, 500 and 6940 elements were created in the model for the modelling of the adhesive layer and the adherends, respectively. Using the built-in kinematic coupling in Abaqus, the left side of the SLJ was fixed in all degrees of freedom while the right side was only allowed to move in the x-direction.

The adherends followed the elastic fully plastic constitutive equations, readily accessible in Abaqus. Following the research in [19], the fatigue damage model was applied to the adhesive layer, where the bi-linear traction-separation response deteriorated. It was implemented in two steps. The peak fatigue load was applied within a static step followed by the cyclic loading in the second step. The constitutive equations employed in these steps were explained in the next.

The displacement jump λ was defined in terms of the separation in Δ_{normal} (Mode 1) and Δ_{shear} (Mode 2) in the bi-linear traction-separation law as follows:

$$\lambda = \frac{K_{shear}{\Delta_{shear}}^2 + K\langle\Delta_{normal}\rangle^2}{\sqrt{{K_{shear}}^2{\Delta_{shear}}^2 + K^2\langle\Delta_{normal}\rangle^2}} \quad (1)$$

The Macauley operator was used for Δ_{normal} to ignore negative values. The relationship between K and K_{shear} is given by

$$\frac{K_{shear}}{K} = \frac{G_{normal,c}}{G_{shear,c}} \left(\frac{\tau_{shear,c}}{\tau_{normal,c}} \right)^2 \tag{2}$$

For each displacement jump for an individual mode, the starting values were required and calculated as follows:

$$\Delta^0_{normal} = \frac{\tau_{normal,c}}{K} \qquad \Delta^0_{shear} = \frac{\tau_{shear,c}}{K_{shear}} \tag{3}$$

The onset displacement jump (λ^0) and critical displacement jump (λ^c) were calculated as follows:

$$\lambda^0 = \sqrt{\frac{K\langle \Delta_{normal} \rangle^2 + \left[K_{shear} {\Delta_{shear}}^2 - K(\Delta^0_{normal})^2 \right][B]^n}{K_B}}$$
$$\lambda^c = \frac{K\Delta^0_{normal}\Delta^c_{normal} + [K\Delta^0_{shear}\Delta^c_{shear} - K\Delta^0_{normal}\Delta^c_{normal}][B]^n}{K_B \lambda^0} \tag{4}$$

Here $\Delta^c_i = 2 * G_{i,c}/\tau_{i,c}$. K_B equals to $K(1-B) + BK_{shear}$, proposed by Turon et al [20]. n represens the material constant used in Benzeggagh-Kenane criterion [21]. B is calculated by

$$B = \frac{K_{shear} {\Delta_{shear}}^2}{K_{shear} {\Delta_{shear}}^2 + K {\Delta_{normal}}^2} \tag{5}$$

To ascertain if the displacement jump was significant enough to damage the adhesive layer, a damage threshold was considered. It was calculated at the present and following increments as follows:

$$r^t = \frac{\lambda^0 \lambda^c}{\lambda^c - D^t_{static}[\lambda^c - \lambda^0]}$$
$$r^{t+1} = \max\{r^t, \lambda\} \tag{6}$$

Here, D^t_{static} was calculated by:

$$D^{t+1}_{static} = \frac{\lambda^c (r^{t+1} - \lambda^0)}{r^{t+1}(\lambda^c - \lambda^0)} \tag{7}$$

The Turon et al.'s [22] fatigue damage model was adapted here. In the fatigue analysis, the load was kept unchanged after it reached to a maximum value in the previous static step.

The following equations were used by the fatigue damage model to relate $\partial D/\partial N$ to da/dN:

$$\frac{\partial D}{\partial N} = \frac{\partial D}{\partial l_d} \frac{\partial l_d}{\partial N}$$
$$\frac{\partial l_d}{\partial N} = \frac{l^e}{l_{CZ}} \frac{da}{dN} \tag{8}$$

where l_{CZ}/l^e was the ratio representing the number of elements in the cohesive zone. The study of Turon et al. [22] suggested the following for l_d/l^e:

$$\frac{l_d}{l^e} = \frac{d\Delta^0}{\Delta^f(1-d) + d\Delta^0} \tag{9}$$

When the Eqs. 7 and 8 were combined together the following was obtained:

$$\frac{\partial D}{\partial N} = \frac{1}{l_{CZ}} \frac{(\Delta^f(1-d) + d\Delta^0)^2}{\Delta^f \Delta^0} \frac{da}{dN} \tag{10}$$

l_{CZ} was calculated for the mixed mode as $l_{CZ} = (9\pi/32)(E_m G_c/(\tau_c)^2)$ [23]. Using the Benzegaggh-Kenane Criterion, G_c was determined as $G_c = G_{normal,c} + (G_{shear,c} - G_{normal,c})[B]^n$. The mixed-mode interlaminar strength τ_c was calculated as ${\tau_c}^2 = {\tau_{normal,c}}^2 + ({\tau_{shear,c}}^2 - {\tau_{normal,c}}^2)[B]^n$. E_m equalled to E due to isotropy of the aluminum adherends. The crack growth rate was defined as $da/dN = C.\Delta G^m$ with $\Delta G = G_{max}(1-R^2)$, where R accounted for the ratio of the minimum and maximum loads during the fatigue loading. The following form is required for the crack to expand steadily: $G_{th} < G_{max} < G_C$, i.e. if the strain energy release rate was more than G_C, the crack development rate would become unstable; while if it was less than G_{th}, the crack could not propagate. G_{max} is calculated as follows:

$$G_{max} = \frac{\tau_{normal,c}}{2}\left[\lambda^f - \frac{(\lambda^f - \lambda_{max})^2}{(\lambda^f - \lambda^0)}\right] \tag{11}$$

A cycle jump strategy was followed in the calculations to cut down on lengthy calculations due to big number of cycles following the study of Van Paepegem and Degrieck [24]. The damage variable at time step $i + \Delta N_i$ was calculated using:

$$D_{i+\Delta N_i} = D_i + \frac{\partial D_i}{\partial N}\Delta N_i \tag{12}$$

ΔN_i influenced the accuracy of the results and was obtained as

$$\Delta N_i = \frac{\Delta D_{max}}{\frac{\partial D_i}{\partial N}} \tag{13}$$

Here, ΔD_{max}, the maximum damage increase, was selected to be 0.005, where such a smaller value resulted in more precise results [25]. Ultimately, the total damage equalled to summation of static and fatigue damages, $D_{total} = D_{static} + D_{i+\Delta N_i}$. With regards to the invoke of different failure modes, a cohesive zone length and a mode-dependent penalty stiffness were calculated following the study of Turon et al. [26]

All the above constitutive equation were accommodated in the computations using a UMAT subroutine [27]. The constants added to Abaqus to simulate the behavior of adherends and the adhesive layer are listed in Table 1.

Table 1. The material constants for the adherends and adhesive layer used in numerical analyses [11].

Parameter	Value	
Material	**AA2024-T3**	**DP460**
E	72400 MPa	-
K	-	10^{14} N/mm^3
ϑ	0.33	0.38
σ_Y	324 MPa	-
$\tau_{i,c}$, i = *normal, shear*	-	32.6 MPa, 28.5 MPa
$G_{i,c}$, i = *normal, shear*	-	2.56 N/mm, 11.71 N/mm
C	-	10^{-12} N/mm^3
m	-	2.0
ΔD_{max}	-	0.005
n	-	2.1

3. Result and discussion

In this section, the numerical model was first validated using experiments from the literature. The impact of adherend thickness on the progression of damage in the adhesive layer was then thoroughly examined.

Numerically obtained number of cycles to failure from the SLJs depending on the amount of load applied (ranging from 3250 N to 1500 N with 250 N decrement) as well as the corresponding stresses applied (ranging from 43.33 MPa to 13.33 MPa) for different adherend thicknesses (3 mm, 4.5 mm and 6 mm) were shown in Fig. 2(a) and Fig. 2(b), respectively. Table 2 demonstrates the respective number of failure cycles. The experimental values taken from Ref. [11] were also presented in both figures. They were for 3 mm and 6 mm adherend thicknesses with 3000 N and 2500 N loads with the corresponding stresses applied. Overall, a judiciously good agreement of the experiments and simulations was achieved. Only, for the thicker adherends subjected to 2500 N load, the experimentally obtained failure cycles, ranging from 117059 to 198275, were less than the numerically predicted one, 386850 cycles.

It was observed that for the identical fatigue load applied, the SLJs of 3 mm adherends failed at earlier cycles when compared to those of 4.5 mm and 6.0 mm. For instance, for the fatigue load of 3250 N, they were 24610, 33396 and 45953 cycles for adherend thicknesses of 3.0 mm, 4.5 mm and 6.0 mm, respectively, while for 2500 N, the SLJs failed at 101870, 171160 and 386850 cycles, respectively (Table 2). Obviously, the life of SLJs lasted longer when the applied load was reduced. Here, the failure cycle of SLJ of 3 mm increased almost 4.13 times when the load was decreased from 3250 N to 2500 N, whereas it was 8.41 times from for that of 6 mm. It was concluded that the SLJs of thicker adherends were more sensitive to amount of load applied in terms of its service life when compared to those of thinner ones.

The influence of change in the applied load level on the life span of the SLJ was also investigated. When the applied load was decreased by 7.69% from 3250 N to 3000 N, the life of SLJ with 3.0 mm increased by 53.8% from 37857 to 24610 cycles. On the other hand, for a decrease of the loading by 12.5% from 2000 N to 1750 N, more than 100% increase in number of failure cycle was noticed. This revealed that the life span of the SLJs changed more dramatically when subjected to lower amount of load.

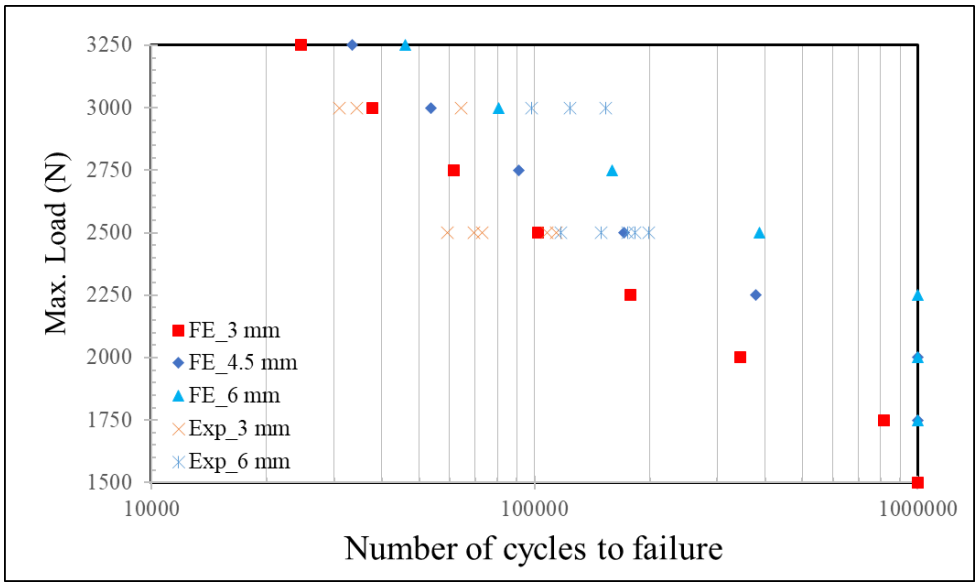

(a)

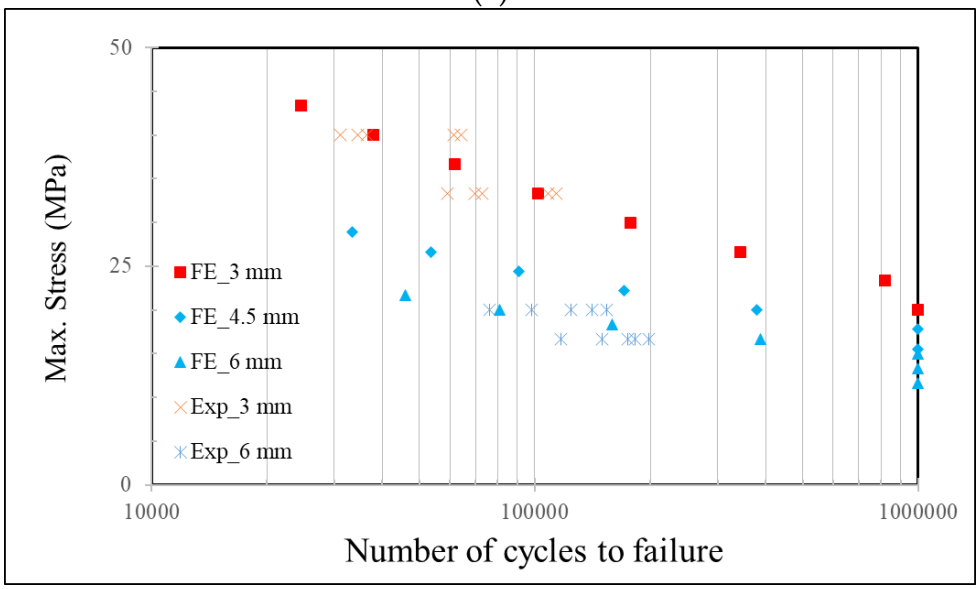

(b)

Figure 2. Experimentally and numerically obtained N_f from the SLJs for various adherend thicknesses when exposed to different loadings (a) and stresses (b).

In the above, the life of SLJs of thicker adherends was found to be longer than those of thinner ones for an identical fatigue load applied. In fact a more fair comparison could be done when the amont of load per cross-sectional area of the adherend, i.e. the stress applied, was considered as a reference. Here, number of failure cycles for different SLJ configurations were compared for the identical applied stress value of 20.00 MPa. They were found to be 1000000 (i.e. no failure), 378670 and 80748 cycles for the adherend thicknesses of 3.0 mm, 4.5 mm and 6.0 mm, respectively. From that respect, the fatigue performance of the SLJ of 3.0 mm adherend was more enhanced than that of 6.0 mm with an infinite life.

Table 2. Life to damage initiation (N_i) and number of cycles to failure (N_f) with their ratios (N_i/N_f) for the SLJs with various adherend thicknesses when exposed to different loadings and stresses.

	***Life to damage initiation* / Number of cycles to failure (their ratio)**

Load (N)	Stress for 3.0 mm (MPa)	Stress for 4.5 mm (MPa)	Stress for 6.0 mm (MPa)	3.0 mm	4.5 mm	6.0 mm
3250	43.33	28.89	21.67	*3135*/**24610**(.127)	*5141*/**33396**(.154)	*7022*/**45953**(.153)
3000	40.00	26.67	**20.00**	*4133*/**37857**(.109)	*5862*/**53712**/(.109)	*9299*/**80748**/(.115)
2750	36.67	24.44	18.33	*5937*/**61728**(.096)	*8256*/**91064**/(.091)	*14023*/**159330**/(.088)
2500	33.33	22.22	16.67	*6393*/**101870**(.063)	*9980*/**171160**/(.058)	*22077*/**386850**/(.057)
2250	30.00	**20.00**	15.00	*9235*/**177520**(.052)	*13503*/**378670**/(.036)	**1000000**
2000	26.67	17.78	13.33	*17177*/**344120**(.050)	**1000000**	
1750	23.33	15.56	11.67	*28994*/**817550**(.035)		
1500	**20.00**	13.33	10.00	**1000000**		

The fatigue load limit was also compared for the SLJs with different configurations. The fatigue load limitations were observed to be 1500 N, 2000 N, and 2250 N, respectively, for the adherend thicknesses of 3.0 mm, 4.5 mm, and 6.0 mm, when a fatigue life greater than 10^6 cycles was used as the run-out. On the other hand, the corresponding fatigue stress limits were 20 MPa, 17.77 MPa and 15.0 MPa, respectively. It was noticed that an increase in the adherend thickness led to a rise in the fatigue load limit [11, 28], whereas a decrease in the fatigue stress limit.

Fig. 3 presents the distribution of the damage variable on the adhesive layer upon the static loading applied and at different fatigue cycles, namely $N_f/4$, $2N_f/4$ and N_f for 3.0 mm adherend thickness and 3250 N fatigue load. As the stresses reached their peaks at the both ends of the adhesive layer upon the static loading applied at the beginning, the damage started in these regions (see Fig. 3 (a)). With the course of fatigue loading, the damage started to propagate, i.e. the crack began to spread evenly from the edges of the adhesive layer towards its center (Fig. 3 (b,c)). After a certain number of failure cycles, all parts of the adhesive layer were damaged (Fig. 3 (c)).

The assessment of a crack initiation is critical and one of the important parameters needs to be considered for a reliable design of a SLJ. Table 2 presents the number of cycles with damage initiation (N_i) in the adhesive layer. Also their ratios against N_f, i.e. N_i/N_f, were also provided for all the configurations simulated. It was important to mention that the number of cycles at which the damage reached a minimum of 90% at one or both ends of the adhesive layer was used to define the life to crack initiation. It was observed that N_i/N_f decreased with a decrease in the load applied to the SLJ irrespective of the thickness of the adhesive layer. It was concluded that for higher loads, the onset of damage on the adhesive layer considering the failure cycles occurred at later stage. When the fatigue load was reduced, the crack initiation in the adhesive layer took place at earlier stage.

$N = 0$ – Static failure

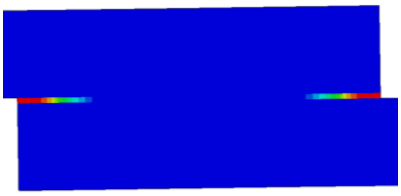

$N = N_f/4$

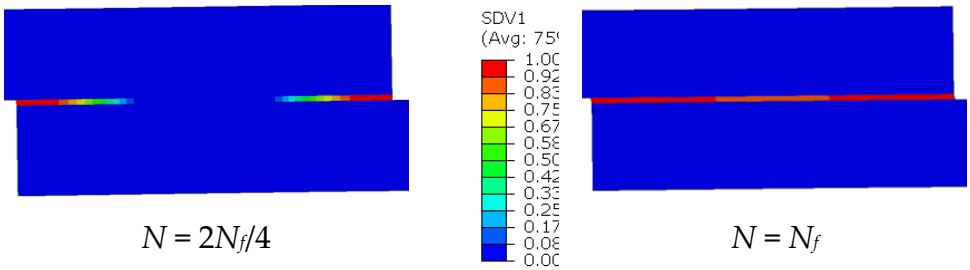

Figure 3. The damage distribution in the adhesive layer along the overlap length at static loading and different fatigue cycles for 3.0 mm adherend thickness (F = 3250 N).

Another vital parameter to evaluate the efficiency of the SLJs is the crack growth rate, da/dN during the fatigue loading. The crack propagation rate vs. number of cycles were compared for different SLJ configurations in Fig. 4. It was observed that the crack propagation rate was not significant at the first cycles since the fatigue damage at the tips of the adhesive layer did not saturate yet, but the damage was still accumulating. After few hundreds of cycles, the crack growth rate started increasing and reached its maximum value steadily followed by a sudden jump at the final stage of the failure. Excluding the unsteady final crack growth regime, the maximum da/dN values were 2.7×10^{-4}, 1.8×10^{-4} and 1.3×10^{-4} mm/cycle for 3 mm adherend thickness when subjected to load values of 3250 N, 3000 N and 2750 N, respectively. The respective values were 6.3×10^{-5}, 3.7×10^{-5} and 2.3×10^{-5} mm/cycle for 6 mm adherend thickness. Firstly, it was noticed that da/dN got larger for smaller adherend thickness. Secondly, the change in da/dN with a change in the applied load to the SLJ was affected by the adherend thickness. For instance, the crack growth rate increased 2.08 times when the load was increased from 2750 N to 3250 N for t = 3.0 mm, while this ratio corresponded to 2.74 for t = 6.0 mm. This result revealed that the sensitivity of crack expansion rate to the applied tensile loading was more prominent for the SLJ with thicker adherends.

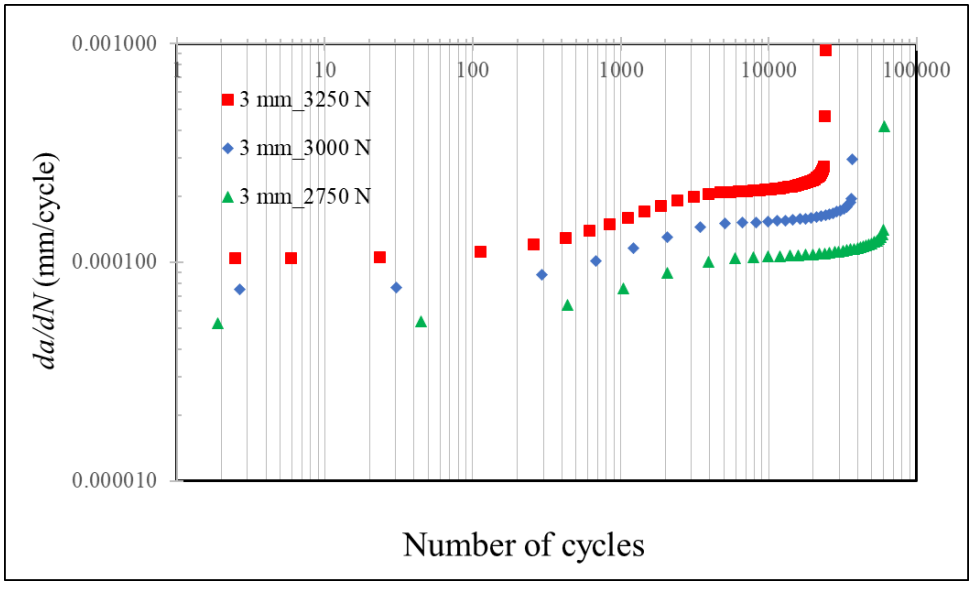

(a)

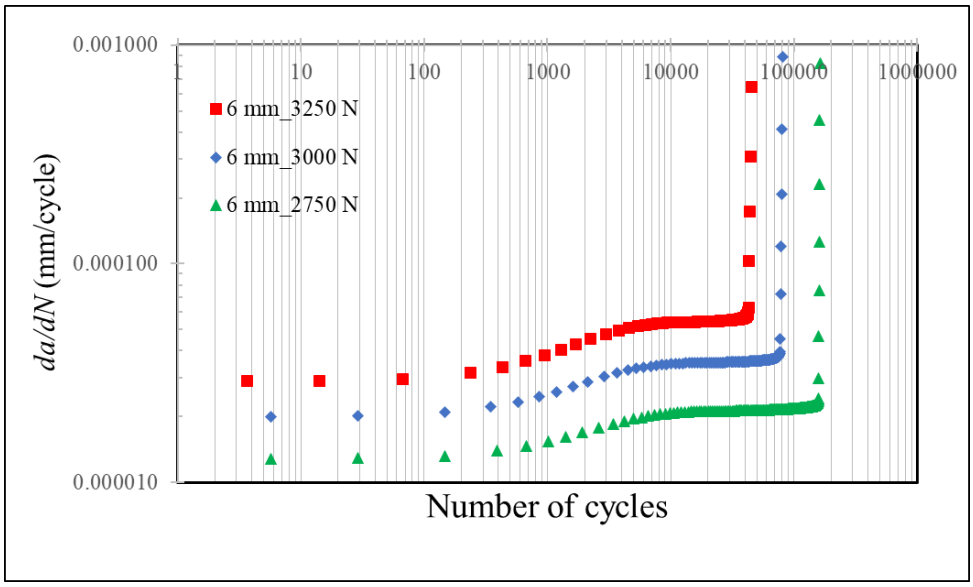

(b)

Figure 4. *da*/*dN* vs. SERR for the SLJ exposed to 2750 N, 3000 N and 3250 N loads for adherend thicknesses of 3.0 mm (a) and 6.0 mm (b).

Fig. 5 compares the *da*/*dN* with respect to the strain energy release rate (SERR) for various loadings and adherend thicknesses. *da*/*dN* vs. SERR was described using the Paris Law in the constitutive equations, where *C* and *m* were identical for the configurations studied here. Thus, all the numerically obtained data fell well on the identical curve. It should be emphasized that these constants were obtained as a result of exhaustive calibration effort, where the predicted failure cycles of SLJs with 3.0 mm and 6.0 mm adherend thicknesses exposed to fatigue loads of 3000N and 2500 N were matched with those obtained experimentally (see Fig. 2).

It was noticed that both *da*/*dN* and SERR became larger for higher fatigue loads (see Fig. 5). It is important to underline that the points denoting the larger values in the plots for both parameters represented the unsteady final crack growth regime. The maximum SERR values were compared for all the relevant configurations excluding the final instable regime. They were 165.7, 138.4, 116.4 J/m^2 when the SLJ was subjected to load values of 3250 N, 3000 N and 2750 N for *t* equalled to 3 mm, respectively. The corresponding values were 82.2, 63.8 and 50.2 J/m^2 for *t* equalled to 6 mm. It was observed that they were larger more than twice for *t* = 3.0 mm in comparison with those of *t* = 6.0 mm for the identical loading. As the SLJ of thinner adherends were exposed to higher load density compared to those of thicker ones, more energy was released for them.

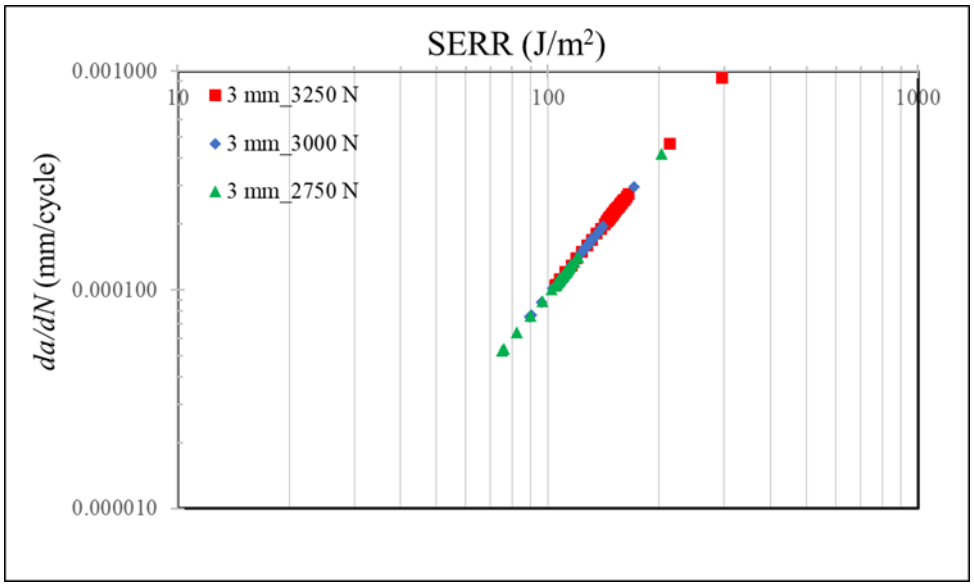

(a)

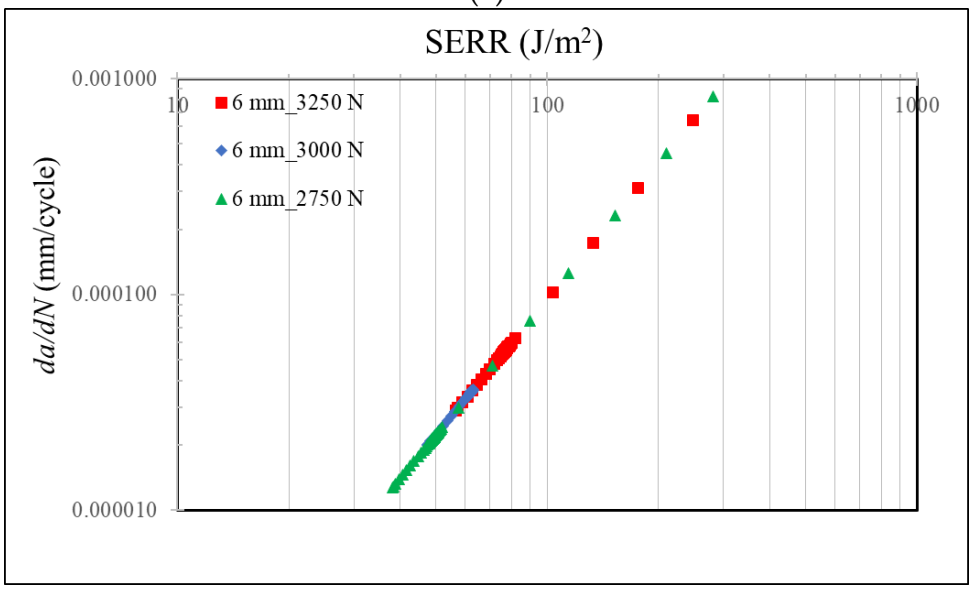

(b)

Figure 5. *da/dN* vs. SERR for the SLJ exposed to 2750 N, 3000 N and 3250 N loads for adherend thicknesses of 3.0 mm (a) and 6.0 mm (b).

In the next section, the effect of adherend thickness and fatigue load applied on the failure mechanisms of the SLJ was investigated. For that purpose, distributions of peel and shear stresses were evaluated. Fig. 6 presents the distributions of S_{13} and S_{33} throughout the overlap length in the adhesive layer with 3.0 mm and 6.0 mm adherend thickness subjected to 2750 N fatigue load at different loading cycles, namely, just after the static loading, $N_f/4$, $2N_f/4$ and $3N_f/4$. When the S_{12} values were checked just after the static loading, they started getting smaller at the ends of the overlap length for t = 3 mm due to the damage in shear mode, while this was yet to start for 6 mm. On the other hand, the S_{22} values were maximum at the tips of the adhesive layer. From this, it was concluded that shear failure were pronounced - rather than the peeling effects - in the damage of the adhesive layer for the static loading applied. When the distributions of S_{12} and S_{22} were compared for t = 3 mm and 6 mm, it was noticed that they were much larger at the end of the overlap length rather than its center for the former thickness, while they were more homogenous with less stress gradients for the latter one. It was concluded that the load

was shared more equally by the material points along the overlap length for larger thickness of the adherends. When the fatigue loading was applied, the damage increased at the both tips of the adhesive layer and finally the complete damage was reached. Then the elements there could not carry any loading and both stress components became zero. When the portion of completely damaged elements were compared for increasing number of cycles from $N_f/4$ to $3N_f/4$, they were increasing. For instance, for $3N_f/4$, while almost 24% (x/L = 0.12) of the overlap region was damaged for t = 3 mm, it was around 16% for t = 6 mm. For this loading cycle, the maximum stress was reached when x/L = 0.25 and 0.20 for t = 3 mm and 6 mm, respectively. In other words 50% of the adhesive layer were not damaged yet for the first thickness and 60% for the second one. It was noted that less portion of the adhesive layer were subjected to the damage for thicker adherends for the identical fatigue loading period.

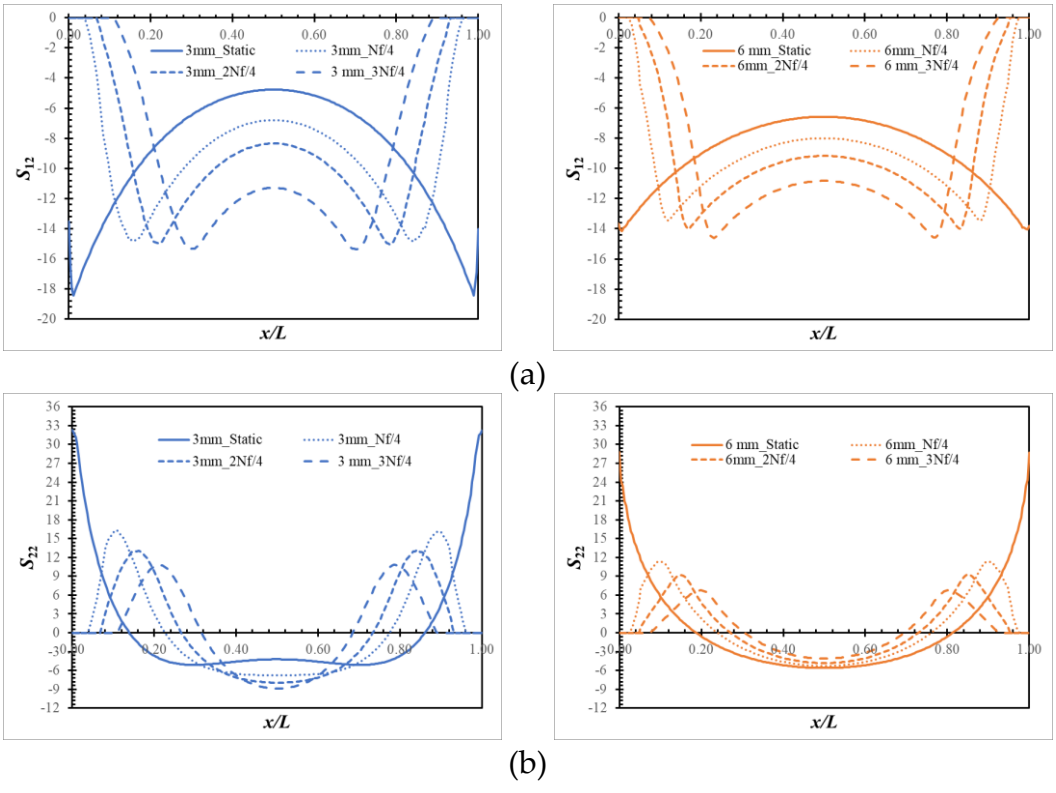

Figure 6. Plot of stress components S_{12} (a) and S_{22} (b) (in MPa) along the overlap length for the SLJs exposed to 2750 N load for adherend thicknesses of 3.0 mm (left) and 6.0 mm (right).

4. Concluding remarks

This study looked into how the fatigue damage evolved in the SLJ's adhesive layer during a tensile test. Its advanced FE model was created for this purpose and tested against the experimental data from the literature. The fatigue damage model, which was then used to predict the behavior of the adhesive layer, was incorporated in the cohesive zone model. From this study, the succeeding conclusions were achieved:

- The SLJs with thicker adherends were observed to be more sensitive to amount of load applied in terms of its service life.
- The life span of the SLJs changed more dramatically when subjected to lower amount of load.
- A smaller thickness of the adherend in SLJ resulted in a decrease in the fatigue load limit, but led to an increase in fatigue stress limit.

- When the fatigue load was increased, the crack initiation in the adhesive layer took place at later stage when considering the failure cycle, i.e. an increased N_i /N_f with shorter crack propagation duration was noticed.
- The crack propagation rate was not significant while the fatigue damage was still accumulating along the overlap length. Afterwards, it started increasing and reached its maximum gradually followed by a sudden jump at the final unsteady stage of the failure. The change in crack propagation rate with a change in the amount of tensile loading applied was less for the SLJ with thinner adherends.
- It was noted that larger share of the adhesive layer were damaged for thinner adherends for the identical fatigue loading period.

Nomenclature

a	crack length
da/dN	crack expansion rate
B	local mixed-mode ratio
C	constant in Paris law
CZ	cohesive zone
D_i, $D_{i+\Delta N_i}$	fatigue damage variables at time step i and $i + \Delta N_i$, respectively
D^t_{static}, D^{t+1}_{static}	static damage at the present and next incements, respectively
D_{total}	total damage
E	Young's Modulus
E_m	mixed-mode Young's Modulus
FE	finite-element
G_c	mixed-mode fracture toughness
G_{max}	area under the traction separation curve
$G_{normal,c}$	critical strain energy release rate for the opening mode
$G_{shear,c}$	critical strain energy release rate for the shear mode
G_{th}	threshold value for the strain energy release rate
K	interface stiffness for the opening mode
K_B	mode dependent penalty stiffness
K_{shear}	penalty stiffness for the shear mode
m	constant in Paris law
l_{CZ}	length of the cohesive zone
l_d	length of the damaged area
l^e	size of the finite element
N_i	crack initiation cycle
N_f	failure cycle
n	material constant used in Benzeggagh-Kenane criterion

R	load ratio
SERR	strain energy release rate
SLJ	single lap joint
UMAT	user material available in Abaqus
λ	displacement jump
λ^0	onset displacement jump
λ^c	critical displacement jump
λ_{max}	maximum displacement jump
$\partial D/\partial N$	fatigue damage evolution variable
$\partial l_d/\partial N$	expansion rate of the length of the damaged area
ΔN_i	skipped number of cycles
ΔD_{max}	selected maximum damage increase in the computations
Δ_{normal}	separation in Mode 1 (opening mode)
Δ_{shear}	separation in Mode 2 (shear mode)
σ_Y	yield strength
$\tau_{normal,c}$	interfacial strength for the opening mode
$\tau_{shear,c}$	interfacial strength for the shear mode
τ_c	mixed-mode interlaminar strength
ϑ	Poisson's ratio
$\langle . \rangle$	Macauley operator

Author Contributions: Conceptualization, Murat Demiral and Salih Akpinar; Methodology, Murat Demiral and Fethi Abbassi; Software, S. Abolfazl Zahedi; Validation, Murat Demiral; Investigation, Murat Demiral, Fethi Abbassi and Salih Akpinar; Writing – original draft, Murat Demiral; Writing – review & editing, Murat Demiral, Fethi Abbassi, S. Abolfazl Zahedi and Salih Akpinar; Supervision, Murat Demiral. All authors have read and agreed to the published version of the manuscript.

Funding: The APC was funded by the American University of the Middle East, Kuwait

Conflicts of Interest: The authors declare no conflict of interest.

References

1. Sioutis I, Tserpes K. A Literature Review on Crack Arrest Features for Composite Materials and Composite Joints with a Focus on Aerospace Applications. Aerospace. 2023 Jan 31;10(2):137.
2. Chowdhury N, Chiu WK, Wang J, Chang P. Static and fatigue testing thin riveted, bonded and hybrid carbon fiber double lap joints used in aircraft structures. Composite Structures. 2015 Mar 1;121:315-23.
3. Adams, R.D., *Strength Predictions for Lap Joints, Especially with Composite Adherends. A Review.* The Journal of Adhesion, 1989. **30**(1-4): p. 219-242.
4. Kadioglu, F. and M. Demiral, *Failure behaviour of the single lap joints of angle-plied composites under three point bending tests.* Journal of Adhesion Science and Technology, 2020. **34**(5): p. 531-548.
5. Zhao, B. and Z.-H. Lu, *A Two-Dimensional Approach of Single-Lap Adhesive Bonded Joints.* Mechanics of Advanced Materials and Structures, 2009. **16**(2): p. 130-159.
6. Abdel Wahab, M., *Fatigue in Adhesively Bonded Joints: A Review.* ISRN Materials Science, 2012. **2012**.
7. Khoramishad, H., et al., *Predicting fatigue damage in adhesively bonded joints using a cohesive zone model.* International Journal of Fatigue, 2010. **32**(7): p. 1146-1158.
8. Ibrahim, G.R., A. Albarbar, and K.F. Brethee, *Progressive failure mechanism of laminated composites under fatigue loading.* Journal of Composite Materials, 2020. **55**(1): p. 137-144.

9. Quaresimin, M. and M. Ricotta, *Life prediction of bonded joints in composite materials.* International Journal of Fatigue, 2006. **28**(10): p. 1166-1176.
10. Shahani, A.R. and S.M. Pourhosseini, *The effect of adherent thickness on fatigue life of adhesively bonded joints.* Fatigue & Fracture of Engineering Materials & Structures, 2019. **42**(2): p. 561-571.
11. Sahin, R. and S. Akpınar, *The effects of adherend thickness on the fatigue strength of adhesively bonded single-lap joints.* International Journal of Adhesion and Adhesives, 2021. **107**: p. 102845.
12. Katnam, K.B., et al., *Load Ratio Effect on the Fatigue Behaviour of Adhesively Bonded Joints: An Enhanced Damage Model.* The Journal of Adhesion, 2010. **86**(3): p. 257-272.
13. Li, W., Zhou, S., Shi, Z., Wang, X. and Hu, P., 2017. *Experimental and numerical analysis on fatigue durability of single-lap joints under vibration loads*. The Journal of Adhesion, 93(3), pp.187-203.
14. Ghabezi P, Farahani M. T*rapezoidal traction–separation laws in mode II fracture in nano-composite and nano-adhesive joints.* Journal of Reinforced Plastics and Composites. 2018 Jun;37(11):780-94.
15. Sam-Daliri, O., Faller, L.M., Farahani, M., Roshanghias, A., Araee, A., Baniassadi, M., Oberlercher, H. and Zangl, H., 2019. *Impedance analysis for condition monitoring of single lap CNT-epoxy adhesive joint*. International Journal of Adhesion and Adhesives, 88, pp.59-65.
16. Ramalho, L.D., Campilho, R.D., Belinha, J.A.O.P. and da Silva, L.F., 2020. *Static strength prediction of adhesive joints: A review*. International Journal of Adhesion and Adhesives, 96, p.102451.
17. Rocha, R.J.B. and Campilho, R.D.S.G., 2018. *Evaluation of different modelling conditions in the cohesive zone analysis of single-lap bonded joints*. The Journal of Adhesion, 94(7), pp.562-582.
18. Systemes, D., *Abaqus 6.14 Documentation. Simulia Co. Providence, RI, USA*. 2014.
19. Belnoue, J. P. H., Giannis, S., Dawson, M., & Hallett, S. R. *Cohesive/adhesive failure interaction in ductile adhesive joints Part II: Quasi-static and fatigue analysis of double lap-joint specimens subjected to through-thickness compressive loading*. International Journal of Adhesion and Adhesives, 2016. **68**: p. 369-378.
20. Turon, A., et al., *A damage model for the simulation of delamination in advanced composites under variable-mode loading.* Mechanics of Materials, 2006. **38**(11): p. 1072-1089.
21. Benzeggagh, M.L. and M. Kenane, *Measurement of mixed-mode delamination fracture toughness of unidirectional glass/epoxy composites with mixed-mode bending apparatus.* Composites Science and Technology, 1996. **56**(4): p. 439-449.
22. Turon, A., et al., *Simulation of delamination in composites under high-cycle fatigue.* Composites Part A: Applied Science and Manufacturing, 2007. **38**(11): p. 2270-2282.
23. Smeets, E. Development of a Fatigue Analysis Tool Using Cohesive Zone Modelling for Composite Specimens. Master's Thesis, Delft University of Technology, Delft, The Netherlands, 2019.
24. Van Paepegem, W. and J. Degrieck, *Fatigue degradation modelling of plain woven glass/epoxy composites.* Composites Part A: Applied Science and Manufacturing, 2001. **32**(10): p. 1433-1441.
25. Demiral, M. and Mamedov, A., 2023. Fatigue Performance of a Step-Lap Joint under Tensile Load: A Numerical Study. Polymers, 15(8), p.1949.
26. Turon, A., et al., *Accurate simulation of delamination under mixed-mode loading using a cohesive model with a mode-dependent penalty stiffness.* Composite Structures, 2018. **184**: p. 506-511.
27. Demiral M, Abbassi F, Muhammad R, Akpinar S. Service Life Modelling of Single Lap Joint Subjected to Cyclic Bending Load. Aerospace. 2023 Jan;10(1):8.
28. Azari, S., M. Papini, and J.K. Spelt, *Effect of adhesive thickness on fatigue and fracture of toughened epoxy joints – Part I: Experiments.* Engineering Fracture Mechanics, 2011. **78**(1): p. 153-162.